May the Shields theory be extended to cohesive and adhesive benthic sediments?

Maurizio Righetti[1] and Corrado Lucarelli[1]

Received 26 April 2006; revised 23 November 2006; accepted 12 December 2006; published 19 May 2007.

[1] A threshold criterion for incipient motion of cohesive-adhesive sediments, based on moment balance and dimensional considerations, is here developed. The criterion discriminates between single particles and flocs critical conditions and induces a modification to the traditional Shields curve, commonly adopted for noncohesive particles. This modification is particularly effective for the smaller size particles but tending to vanish for the larger ones. The proposed approach is validated on the basis of experiments performed on sediment cores, sampled at different depths, from seven lakes with different trophic conditions and organic matter content. The incipient motion conditions are evaluated by means of an original procedure based on image analysis techniques, which enables the entrainment between single particles and flocs to be distinguished. The adhesion force, which is mainly due to the biological activity at the sediment water interface, is estimated following the proposed criterion and it is found to depend on the organic matter content. In particular the cores sampled in the littoral photic zone are characterized by a bell shaped dependence between adhesion coefficient and organic matter content, which is typical for indicators of biological activity of the littoral ecosystems.

Citation: Righetti, M., and C. Lucarelli (2007), May the Shields theory be extended to cohesive and adhesive benthic sediments?, *J. Geophys. Res.*, *112*, C05039, doi:10.1029/2006JC003669.

1. Introduction

[2] Cohesive sediment dynamics are important in many engineering and ecological applications. This is especially true in a lake, where the bottom currents, due to external forces (e.g. wind) can suspend the bottom sediment, enhancing the release of contaminant and nutrient from the bed into the water column. If sedimentary particles belonging to a flat bed are subjected to a current, they can be dislodged and start to move only when the flow velocity reaches a sufficiently high value. The concept of threshold for particle motion or incipient motion condition, as a result of the balance between hydrodynamic forces acting on a particle and stabilizing forces due to gravity and interparticles interaction, is widely accepted both for cohesive and noncohesive sediments. Nevertheless, the difference in the nature of the interactions for the two kinds of sediments, which is also at the basis of distinction between cohesive and noncohesive materials, has to be carefully taken into account when the parameterization of the threshold is faced. Moreover smaller particles tend to aggregate and then be eroded by chunks or flocs and also this aspect has to be appropriately taken into account both in the momentum balance considerations and in the operational criterion adopted for defining the incipient motion conditions.

[3] The present contribution deals with the parameterization of the threshold for natural cohesive-adhesive sediments motion. On the basis of a rational approach, an original formulation of the incipient motion condition is proposed, which can be seen as an extension of the Shields criterion to cohesive-adhesive sediments.

[4] The proposed model has been validated by means of a series of experiments on benthic sediment samples, for which an original criterion for the discrimination between the incipient motion of isolated particles and flocs has been developed.

2. Previous Work

[5] The critical shear stress for the incipient motion of noncohesive sediments can be expressed in dimensionless form:

$$\vartheta_C = \frac{\tau_{0C}}{(\rho_S - \rho)gd} = \vartheta_{C0}(\mathrm{Re}^*) \tag{1}$$

where ϑ_C is the critical Shields parameter, τ_{0C} is the critical bed shear stress, d is the diameter of the sediment grain, g is the gravitational acceleration, ρ_S and ρ are the sediment and fluid density respectively, and Re^* is the particle Reynolds number, defined as $Re^* = (u^*d)/\nu$, where u^* is the critical shear velocity and ν is the kinematic viscosity. Equation (1) was obtained from dimensional analysis and momentum balance considerations performed on a grain belonging to a cohesionless bed. The experiments of *Shields* [1936] have

[1]Department of Civil and Environmental Engineering, University of Trento, Trento, Italy.

0148-0227/07/2006JC003669

investigated carefully the incipient motion conditions, leading to the well-known Shields curve. However, there have been numerous additions, revisions and modifications of the Shields curve since its original publication. *Yalin* [1972] showed that the Shields curve can be expressed as a function of a particle dimensionless characteristic diameter d^*, defined as $d^* = \frac{g\Delta^{1/3}}{\nu^2}\, d$, where $\Delta = \frac{\rho_S - \rho}{\rho}$ is the relative density of the grain. *Brownlie* [1981] suggested the following expression for the function ϑ_{C0}:

$$\vartheta_{C0}(d^*) = 0.22 d^{*-0.9} + 0.06 \exp\left(-17.77 d^{*-0.09}\right) \quad (2)$$

As far as the particle diameter decreases, typically when d is of the order of magnitude of 100 μm or less [*Dade et al.*, 1992; *Lick et al.*, 2004; *You*, 2006], the stabilizing effect of the cohesive forces due to interparticles electrochemical interactions cannot be neglected and plays a dominant role in controlling the incipient motion conditions. *Graf* [1984] applied the momentum balance considerations on fine cohesive particles and proposed the following qualitative expression of the critical Shields parameter ϑ_C:

$$\vartheta_C = \vartheta_{C0} + C_0 \quad (3)$$

where C_0 is defined as a coefficient of cohesion of the material, not quantified by the author, which has to be experimentally evaluated. *Miller et al.* [1977] extended the original Shields curve, which was obtained for $Re^* > 1$, down to $Re^* < 0.05$ and noticed a certain tendency of the incipient motion curves for cohesive materials to sort according to bulk density. This behavior has been noticed by many other authors [see, e.g., *Migniot*, 1968; *Miller et al.*, 1977; *Ohtsubo and Muraoka*, 1986; *Mehta et al.*, 1989; *Krone*, 1999; *Sanford and Maa*, 2001; *Dade et al.*, 1992; *Lick et al.*, 2004]. The theoretical and experimental work of *Israelachvili* [1997] enables the cohesive interparticle forces F_C, which are mainly due to van der Waals interactions, to be quantified, at least for spherical particles. These forces were found to scale with particles diameter:

$$F_C = c \cdot d \quad (4)$$

where the cohesion coefficient c (N/m) depends on the different mineralogies and different coatings on the particle surfaces, as well as on the interparticle distance. The latter dependence explains the fact that the incipient motion conditions of cohesive sediments (and in general their mechanical properties, like the rheology and the erosion rate) are related also to the bulk density of the granular heap. Van der Waals forces have also been directly measured by different authors using an atomic force microscope, these measurements can be useful for the estimation of the critical conditions [see, e.g., *Lick et al.*, 2004].

[6] The problem is far more complicated when binding agents (e.g. polymers or colloidal suspensions such as bentonite) are structurally present in the sediment matrix. In this case, the sediment incipient motion is governed not only by hydrodynamic forces (drag and lift) and by electrochemical forces (van der Waals bonding) but also by binding forces between particles that further enhance aggregation and floc formation [*Walker and Bob*, 2001; *Liwarska-Bizukojc*, 2005]. Therefore, although cohesion is the driving parameter for the initial floc formation process [*Krone*, 1984], aggregate growth is mainly due to adhesion phenomena between contiguous flocs [*Walker and Bob*, 2001; *Liwarska-Bizukojc*, 2005; *Jarvis et al.*, 2005].

[7] The conceptual distinction between cohesive and adhesive interparticle interactions deserve particular attention. *Israelachvili* [1997] defines the cohesive forces at molecular scale as the result of the attractive interactions in vacuum between contiguous particles of the same medium, while the adhesive forces are defined as the additional binding forces between particles, due to the presence of a second, interparticle medium. The physical and chemical characteristics of the interparticle medium obviously mark the strength of the adhesive interactions. We can extend and adapt these definitions to the case of sediment particles saturated with water. In particular we could define cohesion as the result of attractive van der Waals interactions between particles of the same medium, saturated with clear water. Consequently the adhesion can be defined as any additional binding forces due to variation in composition of the second interparticle medium, with respect to the clear water.

[8] *Lick et al.* [2004], gives an illuminating example of the conceptual differences between cohesive and adhesive contribution on the particle stability. They analyzed the incipient motion conditions of fine-grained quartz sediments subjected to a water flow and noticed that the addition of bentonite to the particle interstitial water induces an increase in the critical shear stresses with respect to the values obtained in clear water. They ascribed this stabilizing effect of bentonite to adhesion forces. Based on rational analysis, *Lick et al.* [2004] proposed two different parameterizations for cohesion and adhesion, concluding that interparticle cohesive forces can be estimated following *Israelachvili*'s [1997] approach yielding equation (4) (so scaling with the particle diameter), while adhesive forces scale with the square of the grain diameter.

[9] It is worth remarking that, as a result of interparticles interactions, mineral fine particles tend to aggregate in various orders of clusters of different sizes. Thus, a cohesive sediment bed is not only eroded particle by particle but also as chunks or aggregates of sedimentary particles. This circumstance makes the definition of the critical conditions more complex.

[10] Analogous behavior is evident in benthic sediments where organic matter is the major binding agent. The formation of aggregates appears to be hierarchically organized: primary particles and clay microstructures are bound into microaggregates, which, in turn, are bound into larger macroaggregates [*Jastrow*, 1996; *Krone*, 1999]. As reported for example by *Liao et al.* [2002], an organic floc may be described as initially formed by an internal compact core, in which the cohesive van der Waals interactions are the dominant forces, and by an external shell where other kinds of binding forces take place and tend to prevail. The latter are mainly due to the different biologically-mediated linkages between sediment aggregates such as hydrophilic and/or hydrophobic interactions between flocs surfaces [*Jorand et al.*, 1998; *Donlan*, 2002]. Biological activity is particularly intense at the surface layer of benthic sediments [*Haglund et al.*, 2003] where produces, as a result, a biofilm

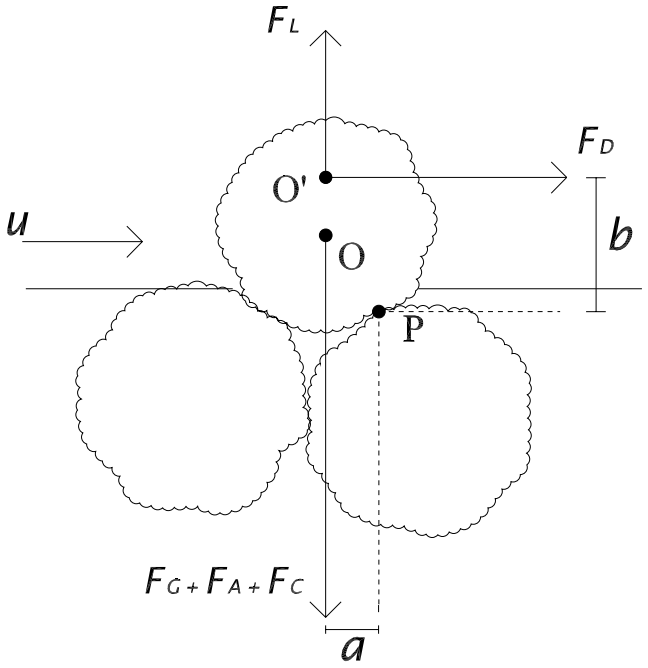

Figure 1. Forces acting on a single floc in fluid flow.

that may glue flocs together, thus promoting the increase of floc size [*Decho*, 1990; *De Winder et al.*, 1999; *Van der Lee and Termaat*, 2000]. This stabilizing effect can therefore be schematized as a biological adhesion force, which induces an increase of the critical shear stress value [*Yallop et al.*, 2003; *De Brouwer et al.*, 2005; *Perkins et al.*, 2004]. The characteristics of such adhesive binding are strongly affected by the biochemical nature and structure of the organic matter [see, e.g., *Wilkinson et al.*, 1997].

[11] It is therefore expected that cohesive forces are significant when the incipient motion of the primary aggregates is considered, becoming negligible, with respect to adhesive forces, when the stability of macroflocs is taken into account [*Krone*, 1984; *Lick et al.*, 2004].

[12] The approach of *Lick et al.* [2004] seems to be particularly promising concerning the role of adhesion and cohesion on the stability of benthic sediments. Nevertheless, some limitations on the applicability of the Lick's threshold criterion has been pointed out [*You*, 2006]. These limits can be ascribed to a nonexhaustive dimensional analysis of the incipient motion of very small, cohesive particles.

[13] In the present paper, an original rational approach to the problem of the incipient motion of cohesive/adhesive sediments is proposed. This is consistent with the dimensional analysis and can be framed in the context of the Shields theory. With the aim of validating the approach, a series of measurements of critical shear stress has been performed. The experiments were made on several samples of benthic sediments taken from seven different alpine lakes. An original method, based on image analysis technique, has been developed for the definition of the incipient motion conditions. The paper is organized as follows: in section 3 the rational approach is explained; section 4 describes the experimental apparatus, the methodology for the tests and the technique developed for the definition of incipient motion conditions; finally section 5 presents and discusses the results and points out the main conclusions.

3. Theoretical Framework for the Definition of Incipient Motion Conditions

3.1. Theoretical Approach

[14] The incipient motion condition of a sediment grain of size d and density ρ_S, belonging to a cohesive-adhesive sediment matrix and exposed to an unidirectional flow, can be studied through the moments equation [*Chepil*, 1959; *Lam Lau and Engel*, 1999]. At initiation of movement of the grain, the balance between the overturning and restoring moments about the rotation point P of the forces acting on the grain, leads to the following equation:

$$F_D b = (F_G + F_C + F_A - F_L)a \tag{5}$$

where F_G is the gravitational force, F_D and F_L the drag and the lift forces, F_C is the cohesive force, F_A is the adhesive force, a and b are the distances of the horizontal and vertical forces to the rotation point (Figure 1), that depend not only on the grain shape but also on the characteristics of the flow field [*You*, 2006].

[15] The grain volume V_P and the grain area projected in the flow direction A_P can be assumed proportional to d^3 and d^2 respectively:

$$V_P = \alpha_3 d^3 \quad A_P = \alpha_2 d^2 \tag{6}$$

with α_2 and α_3 depending on particle shape. In particular, α_3 can be considered equal to about $\pi/6 \cong 0.523$ for near-spherical grains. The drag and lift forces can be assumed proportional to the shear velocity as follows:

$$F_D = C_1 \rho u^{*2} d^2; \; F_L = \eta F_D \tag{7}$$

where C_1 and η are appropriate functions of Re^* [see, e.g., *You*, 2006; *Dade et al.*, 1992; *Lam Lau and Engel*, 1999]. Combining equation (7) with equation (5) and defining the gravitational force F_G as $(\rho_S - \rho)gV_P$, we obtain the following relation:

$$\frac{\tau_{0C}}{(\rho_S - \rho)gd} = \frac{\alpha_3 a/b}{(1 + \eta a/b)C_1}\left(1 + \frac{1}{\alpha_3}\frac{F_C + F_A}{(\rho_S - \rho)gd^3}\right) \tag{8}$$

When cohesion and adhesion are negligible, equation (8) coincides with equation (1), yielding:

$$\vartheta_{C0}(d^*) = \frac{\alpha_3 a/b}{(1 + \eta a/b)C_1} \tag{9}$$

In general, equation (8) can then be rewritten as:

$$\frac{\tau_{0C}}{(\rho_S - \rho)gd} = \vartheta_{C0}(d^*) + \frac{\vartheta_{C0}(d^*)}{\alpha_3}\frac{F_C}{(\rho_S - \rho)gd^3} + \frac{\vartheta_{C0}(d^*)}{\alpha_3}\frac{F_A}{(\rho_S - \rho)gd^3} \tag{10a}$$

that is:

$$\vartheta_C = \vartheta_{C0} + \vartheta_{CC} + \vartheta_{CA} \tag{10b}$$

In order to account for the stabilizing effects of cohesive and adhesive forces, the classical Shields curve, given by $\vartheta_{C0}(d^*)$, must then be corrected by introducing two coefficients ϑ_{CC} and ϑ_{CA}, which represent the additional contributions to the critical Shields parameter due to cohesive and adhesive forces.

[16] It is worth remarking that the proposed approach to the definition of the critical conditions takes into account the cohesive/adhesive characteristics of the sediment together with the hydraulic conditions in the near-bed region and thus complies with dimensional analysis. This circumstance overcomes the limits of application of the threshold criterion proposed by *Lick et al.* [2004], as outlined by *You* [2006], and thus generalizes the Shields criterion to adhesive and cohesive materials.

3.2. Evaluation of Cohesion and Adhesion for a Single Particle

[17] As mentioned above, when single particles with a diameter d and density ρ_S are considered, the cohesive force can be evaluated by means of equation (4), where the cohesion coefficient c can be estimated by means of the Lifshitz theory for the evaluation of van der Waals force between adjacent particles [*Israelachvili*, 1997] (equation (11a)). In this way θ_{CC} takes the expression reported in equation (11b):

$$c \equiv \frac{H}{12r^2} \tag{11a}$$

$$\theta_{CC} \equiv \frac{\vartheta_{C0}(d^*)}{\alpha_3}\frac{c}{(\rho_S - \rho)gd^2} \tag{11b}$$

where r is the separation between contiguous particles, that is the distance between particles surfaces (usually of the order of magnitude of few microns or less) and H (Joule) is the Hamaker constant which also takes into account the influence of neighboring particles on the interaction between pairs of particles [*Israelachvili*, 1997].

[18] In equation (11a) the cohesion coefficient c is expressed as an inversely proportional function to the particles separation. Since the sediment bulk density decreases for increasing particles separation, θ_C is expected to decrease as the bulk density decreases, as is indeed confirmed by nearly all the experiments on incipient motion of cohesive particles.

[19] As far as the adhesive effects are concerned, *Lick et al.* [2004] demonstrated that the adhesion force can be scaled with the square of the particle diameter, that is:

$$F_A = A \cdot d^2 \tag{12a}$$

$$\theta_{CA} \equiv \frac{\vartheta_{C0}(d^*)}{\alpha_3}\frac{A}{(\rho_S - \rho)gd} \tag{12b}$$

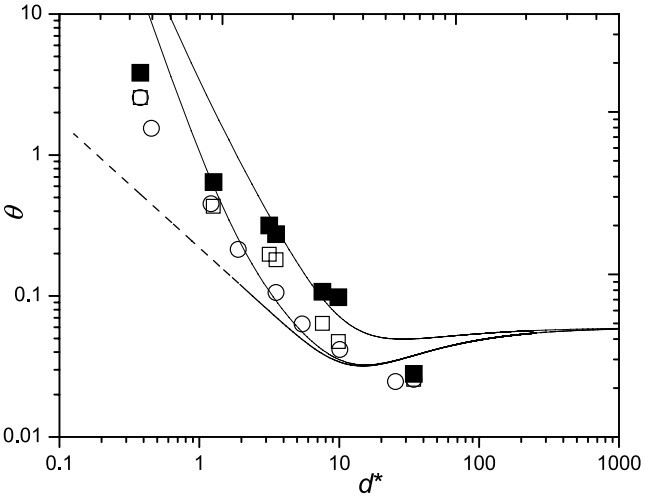

Figure 2. Comparison of theorethical curves and experimental results for incipient motion of quartz particles: dashed curve, Brownlie's curve; solid curve, theoretical curves equation (13) assuming $c = 5 \times 10^{-5}$ N/m, $A = 0$ and $A = 3.5$ N/m^2; open square, quartz particles without bentonite and bulk density 1950 kg/m^3 (only cohesion); open circle, quartz particles without bentonite and bulk density between 1900 and 2000 kg/m^3 (only cohesion); solid square, quartz particles and 2% added bentonite and bulk density between 1900 and 2000 kg/m^3 (cohesion and adesion). Data from *Lick et al.* [2004].

where A is an adhesion coefficient (N/m^2). Thus, replacing equations (11b) and (12b) in equation (10b), the mobility parameters ϑ_{CC} and ϑ_{CA} typical for cohesive and adhesive particles can be obtained. Accordingly equation (10a) takes the following form:

$$\vartheta_C = \frac{\tau_{0C}}{(\rho_S - \rho)gd} = \vartheta_{C0}(d^*) + \frac{\vartheta_{C0}(d^*)}{\alpha_3}\frac{c}{(\rho_S - \rho)gd^2} + \frac{\vartheta_{C0}(d^*)}{\alpha_3}\frac{A}{(\rho_S - \rho)gd} \tag{13}$$

The proposed theoretical framework is tested using the experimental data of *Lick et al.* [2004], as reported in Figure 2. In particular only the data referring to three series of experiments are considered: two series of experiments refer to quartz particles in clear water, while the third series of data refers to quartz particles saturated with water, where 2% bentonite as adhesive agent was added. For all the series the particles diameters range between 15 and 1350 μm. The first series has a bulk density of 1950 kg m^{-3}, for the second and the third series the bulk density is declared to range between 1900 and 2000 kg m^{-3} (so namely 1950 kg m^{-3}), thus the bulk density is kept almost constant in all the considered data. Moreover, the particles density was considered equal to 2650 kg m^{-3}. The dependence of cohesion on the bulk density is removed in these series of data and the difference lies only in the composition of the interstitial fluid. Therefore these data are particularly meaningful in order to assess the sensitivity of the model to the variations in the adhesive phenomena.

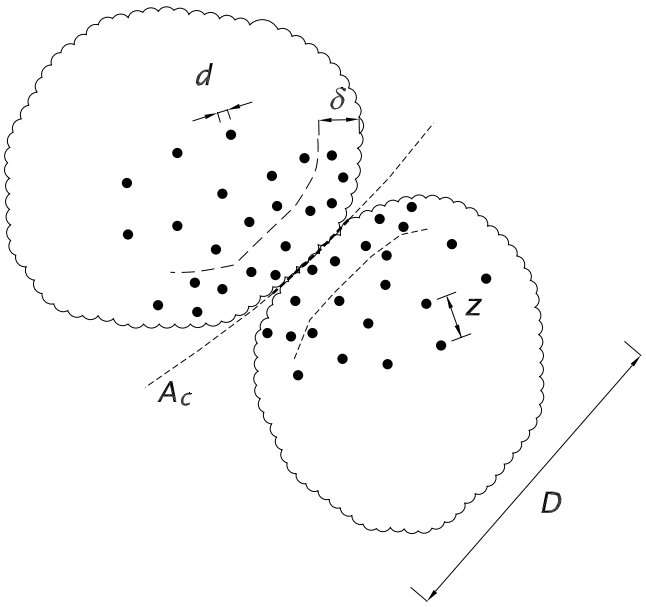

Figure 3. Schematic explanation of the mutual interactions between two contiguous benthic, organic aggregates: d is the mineral particle size, D is the aggregate size, Z is the interparticle distance, δ is the thickness of the external floc shell through which the van der Waals interactions between adjacent flocs are effective, and A_C is the contact area between adjacent flocs.

[20] It is worth noting that the addition of bentonite to quartz particles significantly increases the critical Shields parameter, as a result of induced adhesive stabilizing effects (see Figure 2). However, there are four experimental points that fall below the Shields curve, which have not been considered for the curves fitting.

[21] The experimental data were fitted with the curve equation (13), choosing the cohesion coefficient c value equal to 5×10^{-5} N/m for all the series, while the value of the adhesion coefficient A was chosen equal to 0 N/m (that is, no adhesion effects) and to 3.5 N/m for the 0% (clear water) and for the 2% added bentonite series, respectively.

[22] Figure 2 shows that the curves fit the experimental data in a quite satisfactory way. Moreover, it is worth noting that the corrections to the traditional Shields curve induced by cohesion and adhesion, also reported in Figure 2, tend to vanish with the increase of the dimensionless characteristic diameter d^*, thus leading to negligible cohesive and adhesive effects for the larger particles size. Therefore we can argue that the proposed theoretical model is able to reasonably describe the effects of cohesion and adhesion to the stability of sedimentary particles.

[23] Nevertheless a more detailed analysis of Figure 2 reveals that the chosen values for c and A allow the theoretical curves to fit the experimental data only for the larger particles diameter, while the data corresponding to the smaller ones (namely the experiments with 15 μm particle sizes) fall left of the curves. This discrepancy between the theoretical curves and the experimental evidence is probably due to the occurrence of phenomena of erosion by chunks, not perceived during the experiments, and should not be ascribed to any limit of applicability of the proposed theoretical approach. Indeed, it is well known [see, e.g., *Lick et al.*, 2004] that when cohesive forces are significant -that is for particles small enough- the sediment tends to be eroded not only particle-by-particle but rather by chunks or aggregates, and this tendency increases as the particle size decreases. The explanation of the observed discrepancies calls for a thorough rational analysis of the incipient motion conditions of adhesive-cohesive flocs and also for the set up of an accurate experimental methodology defining the incipient motion conditions. This methodology should be able to distinguish between particles and flocs entrainment. These two aspects will be looked at in the following sections.

3.3. Evaluation of Cohesion and Adhesion Flocs for Benthic Aggregates

[24] The theoretical approach just developed refers to the incipient motion conditions of isolated "small" particles; the situation is a bit different when erosion by chunks or benthic, organic flocs are considered. In this case, as sketched in Figure 3, mineral fine particles of size d and density ρ_S are usually embedded in a biogenic matrix, forming aggregates of size D, the density of these flocs or aggregates can be approximated with the bulk density ρ_B [*Peterson*, 1999]. The evaluation of cohesive-adhesive interactions then deserves a deeper insight. The effective stabilizing van der Waals interactions between adjacent flocs, in fact, act only among particles placed in a thin layer closer to the flocs contact region. The thickness δ of this layer can be estimated at about two or three times the mean interparticles distance Z, while the extension of the contact region A_c can be evaluated as a fraction of the floc surface, being proportional to the square of the floc diameter:

$$\delta = \beta_1 Z; \quad A_C = \beta_2 D^2 \tag{14}$$

where β_1 and β_2 are appropriate coefficients of proportionality. The overall cohesive interaction between adjacent flocs takes the following expression (see Appendix A for details):

$$F_C = \frac{H}{12}\psi\beta_1\beta_2\frac{D^2}{d^3} = CD^2; \tag{15a}$$

$$\vartheta_{CC} = \frac{\vartheta_{C0}(D^*)}{\alpha_3}\frac{C}{(\rho_B - \rho)gD} \tag{15b}$$

where ψ is a coefficient that depends on the bulk density and also on particle density. It has to be pointed out that, unlike the parameterization proposed by *Lick et al.* [2004], the cohesive forces are now proportional to the square of the floc diameter D^2 and not to the particle diameter d. Moreover it should be proven that the coefficient ψ in equation (15a) increases more than proportionally with the bulk floc density ρ_B (see Appendix A). Therefore, in an analogy with what has been found for a single particle, the "constant" C is a function of the bulk density as well and, again, ϑ_{CC} in equation (15b) is expected to decrease as the bulk density decreases, though the dominant effect may be the appearance of bulk density in the denominator of equation (15b) for erosion of flocs.

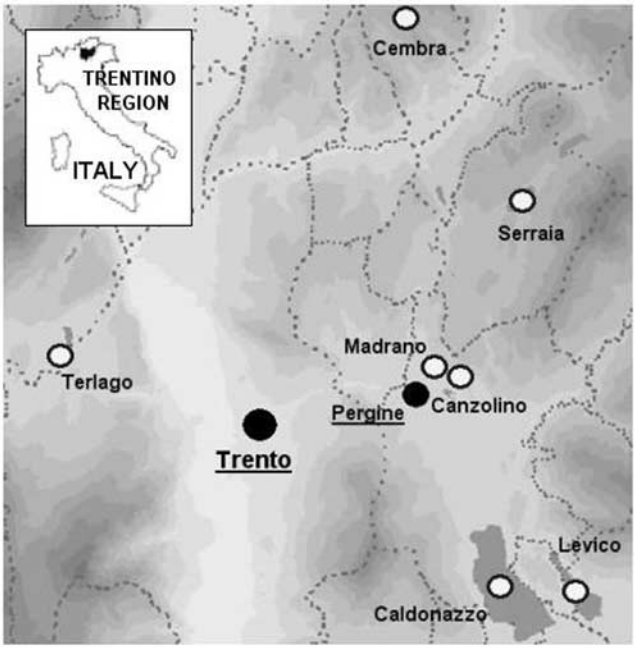

Figure 4. Location of the lakes studied in the Trentino Region, northern Italy.

[25] As far as the adhesive effects are considered, equation (12a) can still be considered valid for benthic sediments also, provided that d is replaced with D. Therefore, when the incipient motion conditions for a floc of size D are considered, equation (10a) can be written in the form:

$$\vartheta_C \equiv \frac{\tau_{0C}}{(\rho_B-\rho)gD} = \vartheta_{C0}(D^*) + \frac{\vartheta_{C0}(D^*)}{\alpha_3}\frac{C}{(\rho_B-\rho)gD} + \frac{\vartheta_{C0}(D^*)}{\alpha_3}\frac{A}{(\rho_B-\rho)gD} \tag{16}$$

4. Materials and Methods

4.1. Sediment Sampling and Analysis

[26] During 2004 and 2005, several series of sediment cores (33) were collected from seven lakes in northeastern part of Trentino (Figure 4 and Table 1) using a gravity corer (ϕ 10 cm). The sampling sites were located both in the littoral zone (depths between 4 and 12 m) and near the deepest point of each lake (depths between 22 and 50 m).

[27] Each series of sediment cores consists of at least 11 cores. Three cores of each series were used to determinate the bulk density ρ_B, the *LOI* ("Loss-on-Ignition", 550°C, 5 hours), which approximates the organic matter content *OM*, and the water content w, of 1 cm slice at the sediment surface, using standard analytical methods [see, e.g., *Jepsen et al.*, 1997]. Sediment morphology and sediment elemental composition were detected at the sediment surface of one more core, by means of a scanning electronic microscope (SEM – EDXS system) JEOL JSM 5500. XRD analysis (Rigaku D/max diffractometer) was also carried out on dried sediments (105°C) for the determination of the main crystalline phases of the analyzed benthic sediment samples. Diffractograms were recorded in the interval 2θ: 10°–80° with a step of 0.05° and an acquisition time of 5s per point.

[28] An optical microscope (Olympus BH, TK-C1381, 50X magnification) was used for the estimation of the size distribution of sediment aggregates located at the surface layer of two more cores. The microscope is provided with a colour CCD-camera (JVC) and a sequence of not less than one hundred images was grabbed for each size distribution analysis. Each image was subsequently analyzed with an interactive Windows application for image processing. After binarizing and thresholding the images, the size of each detected aggregate was evaluated, and the size distribution of all the aggregates detected in the sequence of images was reconstructed. The size of each aggregate is expressed as its mean Feret diameter. The size analysis was also performed for ashed sediments (550°C), in order to evaluate the size of the mineral particles embedded within the aggregates.

[29] Finally, five cores (or more if the size of the series is greater than 11) were used for the evaluation of the critical shear stress in a sedflume, as described in the next section.

[30] Poor quality cores, with a nonlevel surface, and those suffering loss of interface water, were disregarded. All the core samples were carefully stored at 4°C in a field-portable thermostatic chamber, immediately after sampling and during their transport from lake to laboratory. The cores were carefully transported and maintained always covered with at least 3–5 cm of the benthic interface water, in order to minimize the disturbances to the sediments. The cores were analyzed immediately after return to the laboratory: the sediment elemental composition analysis was performed within six hours after the sampling, while the diameter analysis of the fresh samples and the incipient motion tests were performed within three hours after the sampling.

[31] Based on Udden-Wentworth textural classification, the analyzed sediments can be classified as silty loam, but following the Lousiana Geological Survey classification [*Kearns et al.*, 1982], they are classified as mucky clay and/or clayey muck, depending on their organic content.

4.2. Experimental Setup

[32] The critical shear stresses for sediment incipient motion conditions were evaluated by means of tests in a 6 m long, recirculating sedflume. The main structure is shown schematically in Figure 5. The straight plexiglass flume has a rectangular cross section (width 30 cm, high 4 cm) and a test section with an open bottom through which a circular coring tube, containing sediment, can be inserted. The discharge was measured by an electro-magnetic flow-

Table 1. Principal Features of the Studied Lakes[a]

Lake	Elevation	Max Depth	Mean Depth	Area	Trophic State
Caldonazzo	449	49	26.5	5.267	Mesotrophic
Levico	440	38	11.1	1.164	Mesotrophic
Madrano	548	8	4	0.005	Eutrophic
Canzolino	540	15	11.8	0.062	Eutrophic
Cembra	1194	15	5	0.026	Eutrophic
Terlago	414	10	2	0.118	Hypertrohic
Serraia	974	18	6.5	0.452	Hypertrohic

[a]Elevation is in meters a.l.s., depth is in meters, area is in km^2, and trophic classifications are based on the OECD indications (1982).

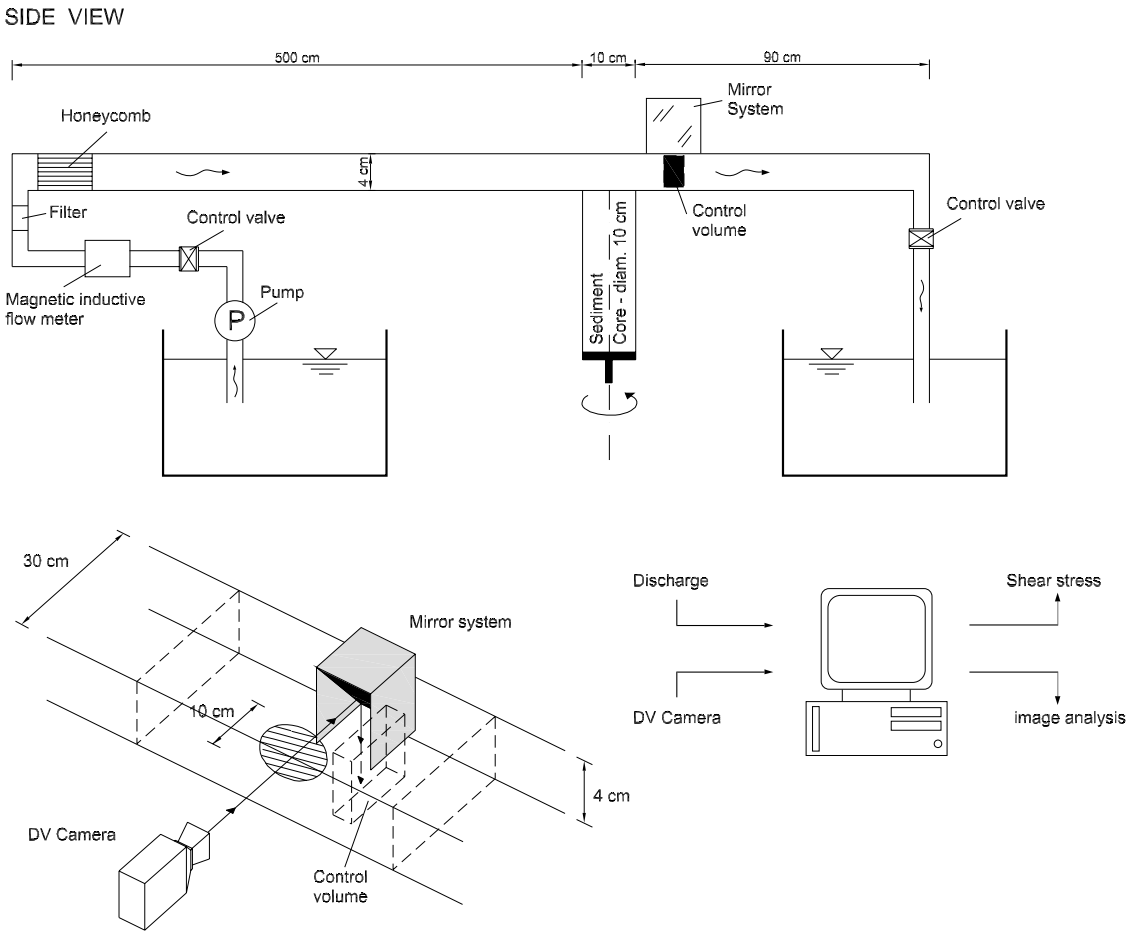

Figure 5. Schematic view of the experimental setup (not to scale).

meter and digitally recorded. The water was pumped through the flume at varying rates and the wall shear stress τ_0 at the sediment-water interface was directly evaluated from the flow rate, according to:

$$\tau_0 = \frac{\lambda}{8}\rho\frac{Q^2}{\Omega^2} \tag{17}$$

where λ is a roughness coefficient evaluated using the Colebrook–White formula, Q is the discharge and Ω the flow cross section area. The shear stresses calculated from equation (17) are in agreement with a series of measurements previously carried out on the same flume at varying flow rates with a 2D laser Doppler anemometer (LDA): the values of τ_0 obtained with equation (17) differ no more than ±15% from the corresponding value evaluated by fitting the Reynolds stress profile obtained with LDA measurements.

[33] An additional piece of equipment for monitoring the particle-floc erosion process was used. A progressive scan DV Camera (Sony DCR-VX2000E, 25 fps, resolution 1px = 150 μm) was mounted at one side of the experimental device (as shown in Figure 5) and a series of mirrors allowed a top view of the flow, just downstream the bottom opening, to be obtained. The camera was fitted with two lamps that illuminate a control volume of the sedflume just downstream of the sediment core. The control volume is 0.022×0.145 m in size. It was thus possible to record the material dislodged from the core by the flow and that passing through the control volume.

[34] Quantification of the critical stage for sediment entrainment was subsequently obtained by automatic image processing. All the recorded images were loaded onto a Windows-based workstation and statistical MatLab® tools were used to carry out the image analysis of dislodged aggregates. Before floc morphologies were analyzed, a number of procedures were enforced, such as eliminating unusuable portions of the image and converting the image to a binary form (Figure 6). In order to distinguish sediment aggregates from the background during the conversion from the original gray-scale to a black-and-white image, the determination of the background light threshold was performed following the approach of *Syvitski and Hutton* [1997].

[35] The developed image analysis procedure enabled the number of detected flocs, their size distribution and their total area, to be elavuated for each recorded image. These data were used to build up a criterion for the definition of the incipient motion conditions, as explained in the next section.

4.3. Methodological Definition of Incipient Motion Conditions

[36] During the experiments, we observed that the surface erosion process of cohesive sediments can be described as a

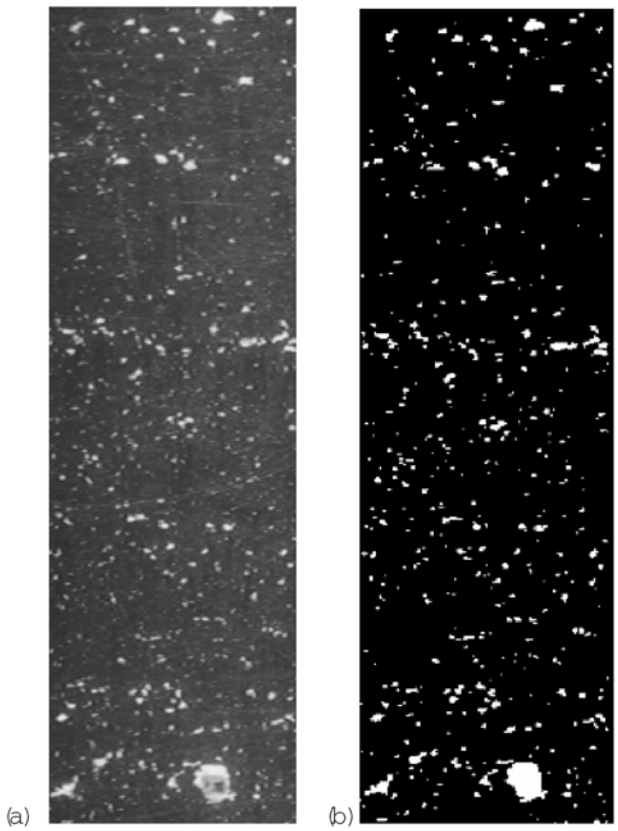

Figure 6. (a) Original DV-Camera image of suspended sediment floc and (b) converted binary image upon which size of each floc is afterwards analyzed.

multistep entrainment phenomenon, for which different stages of sediment motion can be recognized (Figure 7). For low flow velocities, a sporadic, discontinuous motion of aggregates having a relatively small size takes place (Figure 7a). According to *Krone* [1984], these can be regarded as primary particle aggregates weakly bound to floc surfaces. For increasing flow velocities, a more intensive flux of primary particle aggregates is attained, coupled with sporadic entrainment of larger size aggregates. The latter could be regarded as aggregates of higher clustering order (Figure 7b). Further increase in the flow velocity produces, as a results, a gradual enhancement of the flocs entrainment (Figure 7c), until an abrupt change in the erosive process takes place: a sudden increase not only in the quantity of the erodes flocs but also in their size is noticed (Figure 7d). These observations are in qualitative agreement with those reported by many other authors [see, e.g., *Krone*, 1984; *Amos et al.*, 2003; *Lick et al.*, 2004].

[37] Figure 8 shows the time series of the overall area of particle aggregates detected in each frame and the corresponding time series of the wall shear stress values, calculated through equation (17). It has to be pointed out that, during all the tests of incipient motion conditions, the flow velocity was gradually increased in time so that the shear stress growth rate never exceeded $2 \cdot 10^{-3}$ Pa s^{-1}, according to the methodology of *Amos et al.* [2003]. As the shear stress increases, the calculated overall area – which is related to the eroded mass from the core surface – increases according to a quasi-linear trend, until a shear stress threshold is reached, after which a sudden increase in the aggregates area is observed. This sudden increase in size of the eroded aggregates clearly appears also from the time series of the ratio D_{84}/D_{16} of the aggregates size evaluated for each frame (Figure 9).

[38] The critical shear stress τ_{0C} for the incipient motion of larger size aggregates can be defined as the shear stress corresponding to the intersection of the two linear regression curves evaluated for the two erosion regimes, as reported in Figure 8. The aggregate diameter distributions, evaluated for two frames just before and just after the critical shear stress is achieved, are shown in Figures 10a and 10b, respectively. The hystograms comparison clearly shows the increase in size of the detached aggregates as the above defined value of the critical shear stress is achieved. Clearly, in order to correctly evaluate the critical Shields parameter ϑ_C it is necessary to estimate the size D of the macroaggregates which are entrained into suspension (see equation (16)).

[39] Unfortunately, the floc size distribution as measured in a single frame of the video camera is not statistically significant for this purpose due to the paucity of observed flocs. Therefore, a microscope analysis was performed to obtain a reliable size distribution of the sediment aggregates. Each of the two cores used for aggregates size analysis was placed on a vibrating board. The vibration was progressively increased until the aggregate were clearly resuspended in the water overlaying the cores. The overlaying water was then carefully poured into a series of glass microscope trays and the size of the contained aggregates was analyzed through an optical microscope. A typical image of the aggregates is shown in Figure 11a, while the diameter distribution evaluated for a wide sequence of images like the one of Figure 11a is reported in Figure 11b. It can be noted that the shape of the histogram is similar to the one produced from a single frame of the video camera after the incipient motion condition is attained (see Figure 10b). In particular, a bimodal diameter distribution is evident. The reference diameter for the critical Shields parameter of macroaggregates is evaluated by filtering the original distribution with a lognormal high pass filter (see Figure 11b) and by calculating the D_{50} of the filtered distribution.

5. Results and Discussions

[40] The main data obtained from the analysis of benthic lacustrine sediments are summarized in Table 2, where the number of runs for each lake, the critical shear stress τ_{0C}, the ranges of organic matter content, bulk density and benthic aggregate size variations are reported.

[41] The estimated values of the critical shear stress are in good agreement with most of the experimental values obtained by other authors for lacustrine cohesive sediments [see, e.g., *Black et al.*, 2002; *Amos et al.*, 2003].

[42] The XRD analysis performed on the dried sediment samples showed that the mineral fraction of the aggregates is mainly composed of SiO_2 and allumino-silicate (see Figure 12 for an example). The size analysis of the ashed sediments showed that, for all the analyzed samples, the

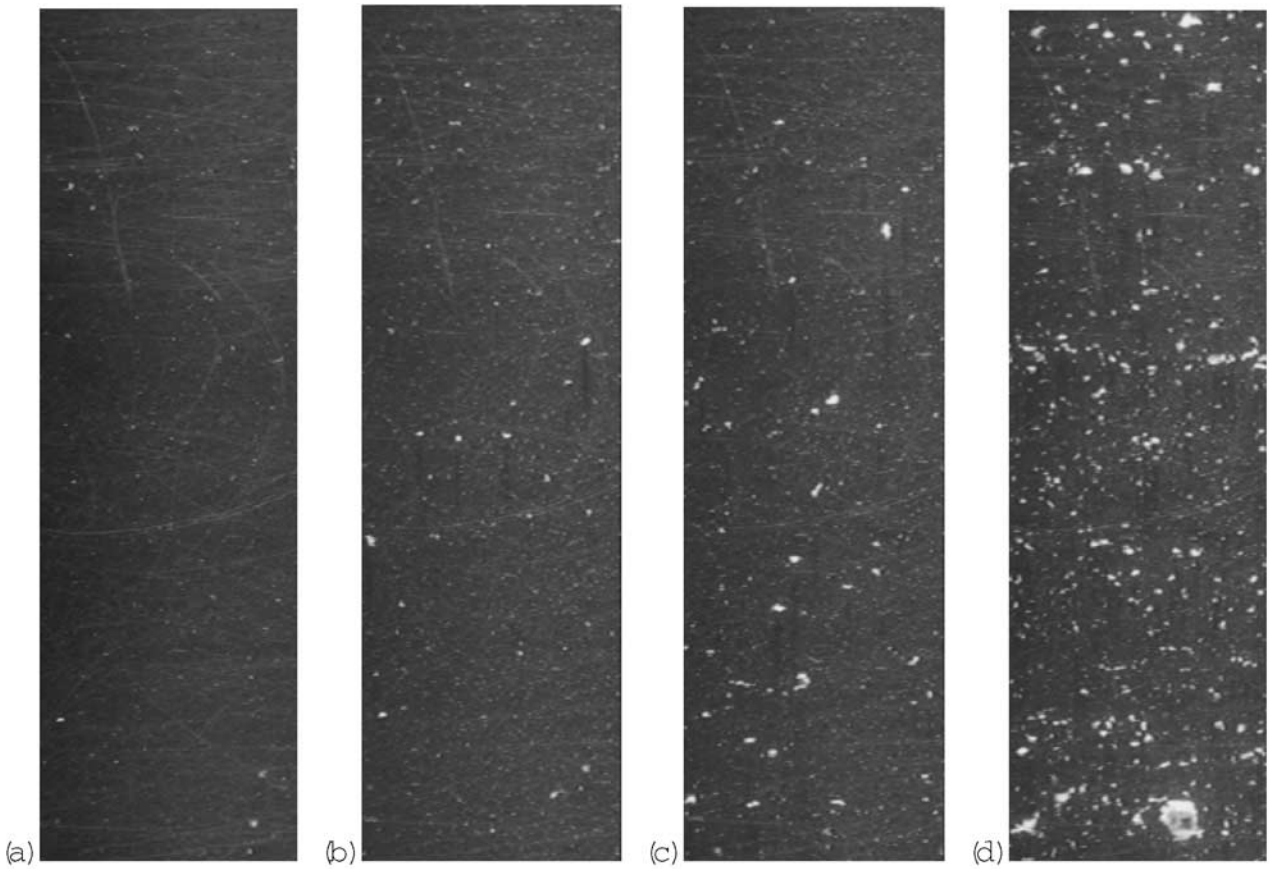

Figure 7. DV Camera images at different steps of the resuspension process at increasing flow rate: (a) initial stage of small size primary particle aggregates erosion at low flow rate; (b) sporadic presence of larger size flocs; (c) enhancement of the flocs erosion; (d) sudden increase in floc erosion at higher flow rate (see also Figure 6). Images refer to one test on sediment core from Lake Terlago.

mineral particles have a mean size of about $4-7$ μm at most. These features allowed us to estimate the value of the Hamaker constant H (assumed equal to $6.5 \cdot 10^{-20}$ J for allumino-silicates) and the value of the particles diameter d to be used in equations (15a), (15b), and (16) for cohesive force evaluation.

[43] Figure 13 shows the values of the critical Shields parameter ϑ_C as experimentally evaluated by the tests of incipient motion in the sedflume. Note that each experimental point reported in the graph refers to one series and is obtained by averaging the values of τ_{0C} measured on five

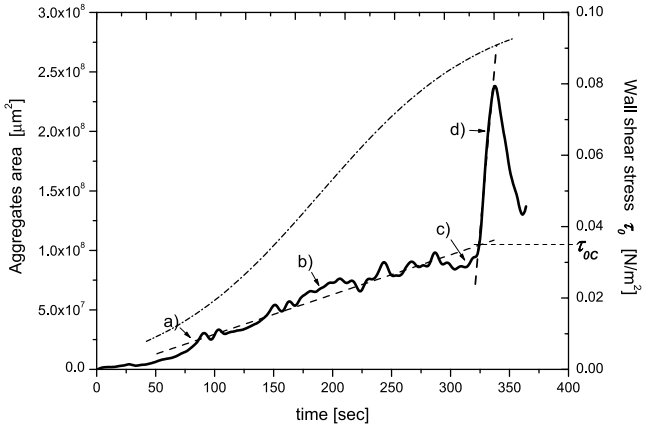

Figure 8. Time series plot for a sediment core erosion process (Lake Terlago): solid curve, total aggregate area for each frame; dashed curve, linear interpolation of different aggregates area time series; dash-dotted curve, wall shear stress; points a, b, c, and d identify the four different motion stages shown in Figure 7.

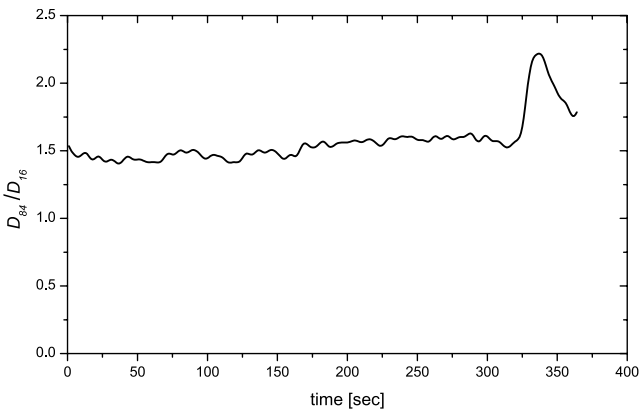

Figure 9. Time series of the ratio 84th to 16th percentile of the aggregates size distribution D_{84}/D_{16}, evaluated for each frame (Lake Terlago).

Table 2. Main Results of the Experimental Investigations Performed on Benthic Sediments[a]

	Number of Runs		Critical Shear Stress τ_{0C}					
Lake	Littoral	Profundal	$\tau_{0C\ min}$	$\tau_{0C\ max}$	$OM_{\ min,max}$	$\rho_{B\ min,max}$	d	$D_{min,max}$
Caldonazzo	8	5	0.094 ± 0.01	0.21 ± 0.02	7.9 – 14.4	1042 – 1157	6	629 – 747
Levico	7	4	0.051 ± 0.005	0.226 ± 0.03	9.9 – 17	1025 – 1132	6	581 – 881
Madrano	1	—	0.063 ± 0.01	0.094 ± 0.05	16.4 – 20.1	1035 – 1057	7	764 – 845
Canzolino	1	—	0.054 ± 0.008	0.08 ± 0.01	21.4 – 25.2	1028 – 1045	6	836 – 888
Cembra	—	1	0.039 ± 0.01	0.059 ± .02	22.1 – 23.9	1032 – 1051	6	829 – 880
Terlago	1	—	0.068 ± 0.01	0.127 ± 0.04	8.1 – 10	1135 – 1175	5	667 – 783
Serraia	5	—	0.044 ± 0.009	0.051 ± 0.01	22.3 – 24.1	1016 – 1022	4	804 – 890

[a] τ_{0C} is in N/m^2 (average value over the cores used for each group); OM is reported as percent loss on ignition; ρ_B is in kg/m^3; mineral particle diameter d and floc diameter D are reported in μm.

different sediment cores. It clearly appears that, due to adhesion and cohesion contribution, the experimental data are located well above the critical conditions suggested by the "traditional" Shields curve valid for noncohesive sediments.

[44] The dimensionless contribution of cohesion and adhesion ($\theta_{CC} + \theta_{CA}$; see equation (10b)), has been evaluated for each experimental point as the difference between the estimated value of ϑ_C and the corresponding value of the noncohesive-nonadhesive contribution ϑ_{C0} estimated with equation (2). Given the value of ($\theta_{CC} + \theta_{CA}$), it is then possible to estimate the sum of cohesion and adhesion coefficients ($C + A$) which appears in equation (16). The order of magnitude of the experimental values ranges between $10^{-1} \div 1$ N/m^2. Moreover an analytical approximate (over)estimation of the cohesion coefficient C by means of equations (15a) and (15b) indicates that C ranges between $10^{-7} \div 10^{-5}$ N/m^2. Therefore the contribution of cohesion forces with respect to adhesion forces on the stability of the macroaggregates can be disregarded. This is in good agreement with the data generally reported in literature [see, e.g., *Krone*, 1984; *Dade et al.*, 1992; *Lick et al.*, 2004].

[45] The experimental values of the dimensionless adhesion coefficient θ_{CA}, as a function of the measured organic matter content values OM, are shown in Figure 14a. It can be seen that no regular trend characterize the data, neither when they are disaggregated, distinguishing between littoral and profundal sediments. On the contrary, Figure 14b shows that the evaluated values of the adhesion coefficient A strongly depends on the OM content and that littoral and profundal sediments exhibit rather different trends.

[46] As far as the littoral sediment are concerned, the adhesive coefficient A assume low values for the lower OM content, increasing up to a maximum when OM ranges between about 10% and 15% LOI, and further decreasing as OM increases. This peculiarity could be explained if the dynamics of the benthic biological activity is taken into account. It is well known that microphytobenthos and bacteria dynamics are tightly related to the OM content [see, e.g., *Hakanson and Jansson*, 1983; *Shimanaga and Shirayama*, 2000]. In particular, according to a widely used model for benthic fauna-organic matter relationship [*Pearson and Rosenberg*, 1978], a given biological variable increases in direct proportion to the organic matter content up to a certain threshold level, for which the biological activity

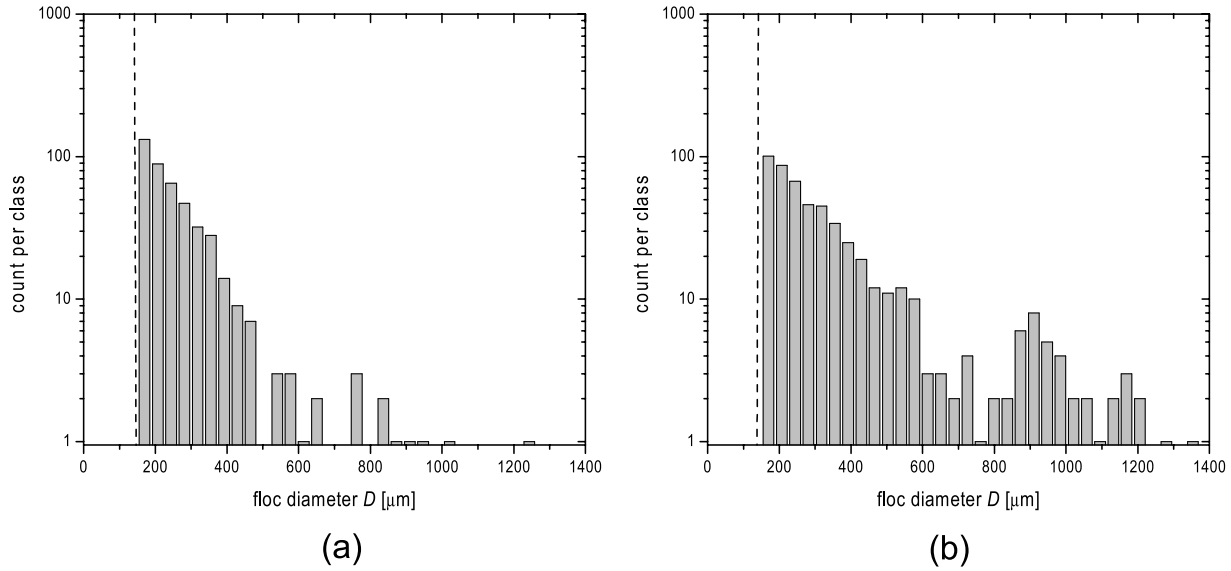

Figure 10. Aggregates size distributions evaluated on two video camera frames, (a) just before and (b) just after the critical condition achievement (corresponding to the points c and d reported in Figure 8). Particles of size less than 150 μm are not reported.

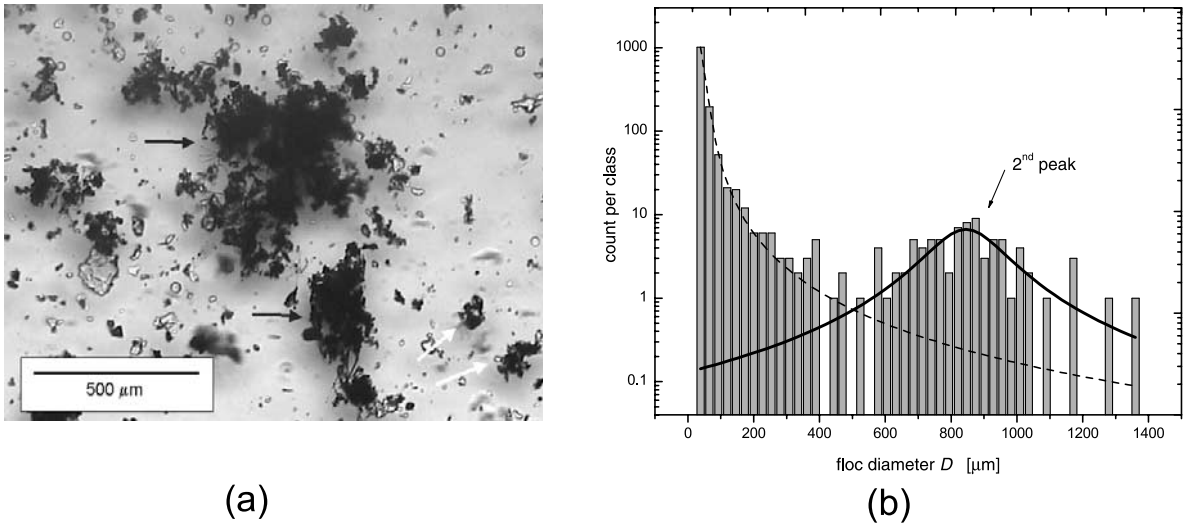

Figure 11. (a) Optical microscope image of benthic sediment aggregates (magnitude 50x), the difference between microaggregates and macroaggregates can be recognized; (b) hystogram of benthic aggregate diameter distribution based on optical microscope analysis. Dashed curve, lognormal high pass filter; solid curve, filtered distribution of flocs.

reach the optimal conditions, and then declines. This behavior is particularly effective when a littoral ecosystem is considered [*Magni*, 2003]. As previously mentioned, the adhesion forces are the result of the biological activity at the sediment-water interface. As a matter of fact, the adhesion coefficient A can be regarded as a particular indicator of this activity, thus exhibiting the tendency to arrange in a bell shaped distribution when plotted as a function of *OM*. On the other hand, the profundal sediments do not show such a trend: the values of adhesion A tend to decrease with *OM* content but the correlation is poor.

[47] This can be explained bearing in mind that the biological activity of the microorganisms at the surface layer of benthic sediments, and hence the physico-chemical properties and the strength of the organic bondings they are responsible for, are driven not only by *OM* content but also by many other physical and biological variables of the system, such as the physico-chemical characteristics of the environment in which the biomass develops [*Hakanson and Jansson*, 1983; *Black*, 1997; *Liao et al.*, 2002; *Liu et al.*, 2004; *Gerbersdorf et al.*, 2005]. Amongst other factors, temperature, oxic-anoxic conditions, irradiance and photoperiod, and its seasonal variance, play a crucial role and

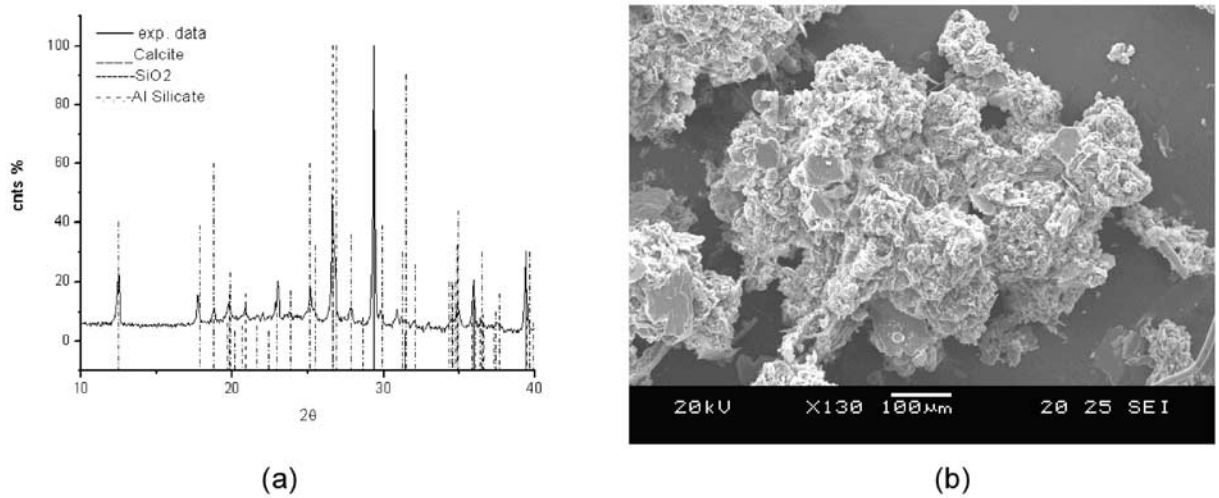

Figure 12. (a) Example of XRD diffractogram for lacustrine benthic sediments (Levico lake): solid line, experimental data; short-dashed line, SiO_2; dashed line, calcite; dash-dotted line, Mg, Al silicate hydrate, K, Mg, Al silicate hydroxide. (b) Scanning electron micrograph of a sediment aggregate showing allumino-silicates particles embedded within sheets and strands of organic substances.

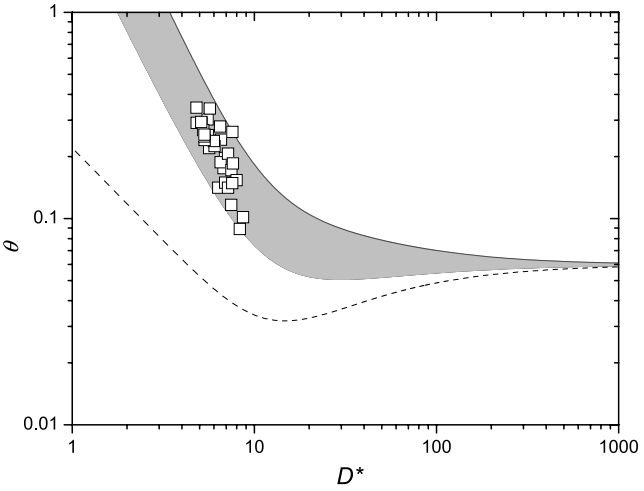

Figure 13. Critical Shields parameter θ_C as a function of D^*: Open squares, experimental data; dashed curve, Brownlie's curve; grey area shows the region in which the experimental data are included.

show strong differences between littoral and profundal environment [*Paterson and Black*, 1999; *De Winder et al.*, 1999; *Friend et al.*, 2003]. Therefore the different response of littoral and profundal sediments to the *OM* content in term of the adhesion coefficient is not surprising.

6. Conclusions

[48] A rational analysis of the incipient motion conditions for cohesive-adhesive sediments has been performed. The stabilizing cohesive and adhesive interactions have been parameterized and a suitably modified critical Shields parameter has been defined. These modifications provide a rational explanation for: (1) the experimental evidence that, in a Shields diagram, the critical conditions for cohesive/adhesive sediments are reached for values of the critical Shields parameter higher than those obtained for noncohesive sediments; (2) the well known dependence of the critical conditions also to the bulk density of the sediments.

[49] Moreover, two different parameterizations of cohesive-adhesive forces have been presented, making a clear distinction between the incipient motion conditions of single particles and that of organic flocs or aggregates. The adopted parameterizations suggest corrections to the traditional Shields curve that are particularly significant for the lower values of the sediment diameter (or, correspondingly, of the grain Reynolds number) and tend to vanish for the higher values. Indeed, increasing the size of sediment particles or aggregates, the adhesion and cohesion forces tend to become negligible with respect to gravitational stabilizing forces.

[50] The theoretical model for the incipient motion of cohesive-adhesive particles has been successfully tested with experimental data of *Lick et al.* [2004].

[51] The theoretical model for the incipient motion of cohesive-adhesive flocs has been used to analyse the incipient motion tests performed on 33 groups of sediment cores (more than 165 core samples) sampled from both littoral and profundal zones of 7 alpine lakes of Trentino Region (Italy). The lakes are characterized by different trophic conditions and different organic matter contents.

[52] The threshold conditions for incipient motion of flocs were experimentally evaluated by means of an original suitable criterion based on image analysis techniques.

[53] The comparison of the experimental data with the theoretical model allowed us to evaluate the contribution of adhesive forces to the critical Shields parameter θ_{CA} and the corresponding adhesion coefficient A.

[54] When the adhesion coefficient A is related to organic matter content, littoral sediments show a different behavior with respect to profundal sediments. For profundal sediments, the values of the adhesion coefficient A tend to decrease with *OM* content but the correlation is poor. On the

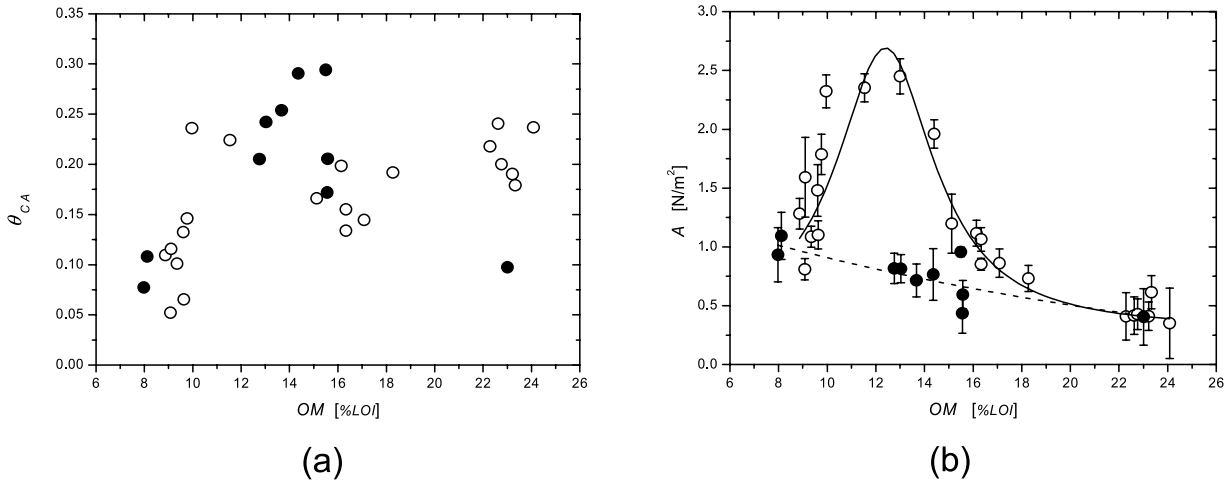

Figure 14. (a) Dimensionless adhesion coefficient θ_{CA} as a function of the measured *OM* values; (b) adhesion coefficient A as a function of *OM*. The data are plotted distinguishing between littoral (open circles) and profundal sediments (solid circles).

other hand, the values of the adhesion coefficient of littoral sediments tend to assume a bell shaped distribution, with maximum values for *OM* in the range 10–15 % *LOI*.

[55] This peculiarity can be explained by observing that the adhesion for natural, benthic sediments is mainly due to the biological activity. Indeed, in the littoral photic zone, biological activity of bacteria and microphytobenthos produces, as a result, extracellular polimeric substances (EPS) that act as a glue between and within adjacent aggregates. It is well known that the biological compartment reaches the optimal conditions only in a certain range of *OM* values. On the other hand, the biological features in the profundal zone, mainly driven by bacterial activity, have a different metabolism depending mostly on the seasonal onset of oxic/anoxic conditions and then the response to OM variation is different.

[56] However, the dependence of the adhesion forces on the bacterial and microphytobenthos biological activity, and in particular on the habitat considered and on its seasonal variations, is still an open question that deserves further investigations.

Appendix A

[57] A sample of natural wet benthic sediment is considered, in which fine mineral particles of size d and density ρ_S are embedded in a biogenic matrix of density ρ_B. W_B is the wet weight of the sample, W_{105} is the dry weight of the oven dried sample (usually 24 h at c.a. 105°C) and W_{550} is the dry weight of the sample after heating to 550 °C for five hours.

[58] The weight of a single mineral particle W_P embedded in the matrix is:

$$W_P = \alpha_3 d^3 \rho_S g \tag{A1}$$

where α_3 is a particle shape coefficient, equal to $\pi/6$ if spherical particle are considered. The number of particles per unit volume of the wet sediment, n_P, is given by:

$$n_P = \frac{W_{550}}{W_B}\frac{\rho_B}{\rho_S}\frac{1}{\alpha_3 d^3} \tag{A2}$$

The mean separation between particle r in the biogenic matrix, for the van der Waals interaction can be evaluated as follows:

$$r = Z - d = n_P^{-1/3} - d = d\left[\left(\frac{W_B}{W_{550}}\frac{\rho_S}{\rho_B}\alpha_3\right)^{1/3} - 1\right] \tag{A3}$$

where Z is the mean interparticles distance, that is the distance between its volume centres.The effective stabilizing van der Waals interactions between adjacent flocs of size D belonging to the sediment matrix (see Figure 3) act only among the mineral particles placed in a thin layer closer to the contact region. The thickness δ of this layer can be estimated at about to be two or three times the mean interparticles distance. The extension of the contact region A_c can be evaluated as a fraction of the floc surface, thus proportional to the floc diameter squared:

$$\delta = \beta_1 Z; \quad A_C = \beta_2 D^2 \tag{A4}$$

where β_1 and β_1 are appropriate coefficient of proportionality.

[59] Therefore an approximate estimation of the overall cohesive interaction between adjacent flocs takes the following expression:

$$F_C = \frac{H}{12(Z-d)^2} d\beta_1 Z \beta_2 D^2 n_P \tag{A5}$$

Introducing equation (A3) in equation (A5) and defining the coefficient ψ as:

$$\psi = \frac{\left(\frac{W_B}{W_{550}}\frac{\rho_S}{\rho_B}\alpha_3\right)^{-2/3}}{\left[\left(\frac{W_B}{W_{550}}\frac{\rho_S}{\rho_B}\alpha_3\right)^{1/3} - 1\right]^2} = \rho_B^{4/3}\frac{\left(\frac{W_B}{W_{550}}\rho_S\alpha_3\right)^{-2/3}}{\left[\left(\frac{W_B}{W_{550}}\rho_S\alpha_3\right)^{1/3} - \rho_B^{1/3}\right]^2} \tag{A6}$$

then equation (A5) can be written as:

$$F_C = \frac{H}{12}\psi\beta_1\beta_2\frac{D^2}{d^3} \tag{A7}$$

[60] **Acknowledgments.** Part of the work was financed by Autonomous Provence of Trento, contract "TREND Project- Study of eutrophication of Caldonazzo lake." The authors were grateful to Dario Montinaro of University of Trento (Italy), Department of Material Engineering and Industrial Technologies, for providing the laboratory XRD analysis, to Cecilia Quintarelli and Stefano Germani of University of Trento (Italy), Department of Civil and Environmental Engineering, for their help during the field measurements. Fruitful discussion with two anonymous referees helped to improve the interpretation and discussion of the results.

References

Amos, C. L., I. G. Droppo, E. A. Gomez, and T. P. Murphy (2003), The stability of a remediated bed in Hamilton Harbour, Lake Ontario, Canada, *Sedimentology*, *50*, 149–168.

Black, K. S. (1997), Microbial factors contributing the erosion resistance in natural cohesive sediments, in *Cohesive Sediments*, edited by N. Burt, R. Parker, and J. Watts. pp. 231–244, Wiley-Interscience, Hoboken, N. J.

Black, K. S., T. J. Tolhurst, S. E. Hagerthey, and D. M. Paterson (2002), Working with natural cohesive sediments, *J. Hydrol. Eng.*, *128*(1), 1–7.

Brownlie, W. R. (1981), Prediction of flow depth and sediment discharge in open channels, *Rep. KH-R-43A*, Calif. Inst. of Technol., Pasadena.

Chepil, W. S. (1959), Equilibrium of soil grains at the threshold of movement by wind, *Soil Sci. Soc. Am. Proc.*, *23*, 422–428.

Dade, W. B., A. R. M. Nowell, and P. A. Jumars (1992), Predicting erosion resistance of muds, *Mar. Geol.*, *105*, 285–297.

De Brouwer, J. F. C., K. Wolfstein, G. K. Ruddy, T. E. R. Jones, and L. J. Stal (2005), Biogenic stabilization of intertidal sediments: the importance of extracellular polymeric substances produced by benthic diatoms, *Microbiol. Ecol.*, *49*, 501–512.

Decho, A. W. (1990), Microbial exopolymer secretions in ocean environments: their role(s) in fodd webs and marine processes, *Oceanogr. Mar. Biol. Annu. Rev.*, *28*, 73–153.

De Winder, B., N. Staats, L. J. Stal, and D. M. Paterson (1999), Carbohydrate secretion by phototrophic communities in tidal sediments, *J. Sea Res.*, *42*, 131–146.

Donlan, R. M. (2002), Biofilms: microbial life on surfaces, *Emerg. Infect Dis.*, *8*(9), 19–38.

Friend, P. L., M. B. Collins, and P. M. Holligan (2003), Daynight variation of intertidal flat sediment properties in relation to sediment stability, *Estuarine Coastal Shelf Sci.*, *58*, 663–675.

Gerbersdorf, S. U., T. Jancke, and B. Westrich (2005), Physico-chemical and biological sediment properties determining erosion resistance of contaminated riverine sediments – Temporal and vertical pattern at the Lauffen reservoir/River Neckar, Germany, *Limnologica*, *35*, 132–144.

Graf, W. H. (1984), Cohesive-material channels, in *Hydraulics of Sediment Transport*, pp. 323–355, McGraw-Hill, New York.

Haglund, A.-L., P. Lantz, E. Toernblom, and L. Tranvik (2003), Depth distribution of active bacteria and bacterial activity in lake sediment, *FEMS Microbiol. Ecol.*, *46*, 31–38.

Hakanson, L., and M. Jansson (1983), Principles of Lake Sedimentology, Springer, New York.

Israelachvili, J. (1997), *Intermolecular and Surface Forces*, 2nd ed., Elsevier, New York.

Jarvis, P., B. Jefferson, J. Gregory, and S. A. Parsons (2005), A review of floc strenght and breakage, *Water Res.*, *39*, 3121–3137.

Jastrow, J. D. (1996), Soil aggregate formation and the accrual of particulate and mineral-associated organic matter, *Soil Biol. Biochem.*, *28*(4/5), 665–676.

Jepsen, R., J. Roberts, and W. Lick (1997), Effects of bulk density on sediment erosion rates, *Water Air Soil Pollut.*, *99*(1), 21–31.

Jorand, F., F. Boue-Bigne, J. C. Block, and V. Urbain (1998), Hydrophobic/hydrophilic properties of activated sludge exopolymeric substances, *Water Sci. Technol.*, *37*(4-5), 307–315.

Kearns, F. L., W. J. Autin, and R. G. Gerdes (1982), Occurrence and stratigraphy of organic deposits, St. Mary Parish, Louisiana, GSA Abstracts With Programs, and Sections, N. E., S. E., Louisiana Geological Survey (LGS), GSA Annual Meeting, Washington, D. C.

Krone, R. B. (1984), The significance of aggregate properties to transport processes, in *Estuarine Cohesive Sediment Dynamics, Lecture Notes on Coastal and Estuarine Studies*, edited by A. J. Metha, Springer, New York.

Krone, R. B. (1999), Effects of bed structure on erosion of cohesive sediments, *J. Hydrol. Eng.*, 1297–1301.

Lam Lau, Y., and P. Engel (1999), Inception of sediment transport on steep slopes, *J. Hydrol. Eng.*, *125*(5), 544–547.

Liao, B. Q., D. G. Allen, G. G. Leppard, I. G. Droppo, and S. N. Liss (2002), Interparticle interactions affecting the stability of sludge flocs, *J. Colloid. Interface Sci.*, *249*, 372–380.

Lick, W., L. Jin, and J. Gailani (2004), Initiation of movement of quartz particles, *J. Hydrol. Eng.*, 755–761.

Liu, Y., Y. Liu, and J. Tai (2004), The effects of extracellular polymeric substances on the formation and stability of biogranules, *Appl. Microbiol. Biotechnol.*, *65*, 143–148.

Liwarska-Bizukojc, E. (2005), Application of image analysis techniques in activated sludge wastewater treatment processes, *Biotechnol. Lett.*, 1427–1433.

Magni, P. (2003), Biological benthic tools as indicators of coastal marine ecosystems health, *Chem. Ecol.*, *19*(5), 363–372.

Mehta, A. J., E. J. Hayter, R. Parker, R. B. Krone, and A. M. Teeter (1989), Cohesive sediment transport. I: process description, *J. Hydrol. Eng.*, *115*(8), 1076–1091.

Migniot, C. (1968), Étude des propriétés physiques des differents sediments très fins et de leur comportement sous des actions hydrodynamiques, *Houille Blanche*, *7*, 591–620.

Miller, M. C., I. N. McCace, and P. D. Komar (1977), Threshold of sediment motion under unidirectional currents, *Sedimentology*, *24*, 507–527.

Ohtsubo, K., and K. Muraoka (1986), Re-suspension of cohesive sediments by currents, paper presented at Third International Symposium on River Sedimentation, Univ. of Miss., Jackson.

Paterson, D. M., and K. S. Black (1999), Water flow sediment dynamics and benthic biology, *Adv. Ecol. Res.*, *29*, 155–193.

Pearson, T. H., and R. Rosenberg (1978), Macrobenthic succession in relation to organic enrichment and pollution of the marine environment, *Ocean. Mar. Biol.*, *16*, 229–311.

Perkins, R. G., D. M. Paterson, H. Sun, J. Watson, and M. A. Player (2004), Extracellular polymeric substances: quantification and use in erosion experiments, *Cont. Shelf Res.*, *24*, 1623–1635.

Peterson, E. L. (1999), Benthic shear stress and sediment condition, *Aquacult. Eng.*, *21*, 85–111.

Sanford, L. P., and J. P. Y. Maa (2001), A unified erosion formulation for fine sediments, *Mar. Geol.*, *179*, 9–23.

Shields, A. (1936), Application of similarity principles and turbulence research to bed-load movement, report, translated by W. P. Ott and J. C. van Uchelen, Calif. Inst. of Technol., Pasadena.

Shimanaga, M., and Y. Shirayama (2000), Response of benthic organisms to seasonal change of organic matter deposition in the bathyal Sagami Bay, central Japan, *Oceanol. Acta*, *23*(1), 91–107.

Syvitski, J. P. M., and E. W. H. Hutton (1997), Floc: image analysis of marine suspended particles, *Comput. Geosci.*, *23*, 967–974.

Van der Lee, W. T., and R. Termaat (2000), The settling of mud flocs in the Dollard estuary, dissertation, Univ. of Utrecht, Utrecht, Netherlands.

Walker, H. W., and M. M. Bob (2001), Stability of particle flocs upon addition of natural organic matter under quiescent conditions, *Water Res.*, *35*(4), 875–882.

Wilkinson, K. J., J. C. Negre, and J. Buffle (1997), Coagulation of colloidal material in surface waters: the role of natural organic matter, *J. Contam. Hydrol.*, *26*, 229–243.

Yalin, M. S. (1972), *Mechanisms of Sediment Transport*, Elsevier, New York.

Yallop, M. L., D. M. Paterson, and P. Wellsbury (2003), Interrelationships between rates of microbial production, exopolymer production, microbial biomass, and sediment stability in biofilms of intertidal sediments, *Arch. Environ. Contam. Toxicol.*, *45*(1), 116–126.

You, Z. J. (2006), Discussion of "Initiation of movement of quartz particles" by Wilbert Lick, Lijun Jin, and Joe Gailani, *J. Hydrol. Eng.*, 111–112.

C. Lucarelli and M. Righetti, Department of Civil and Environmental Engineering, University of Trento, 38050 Trento, Italy. (corrado.lucarelli@ing.unitn.it; maurizio.righetti@ing.unitn.it)